

Article

Terahertz Metamaterial Modulator Based on Phase Change Material VO₂

Yanfei Dong ¹ , Dingwang Yu ^{1,2,*}, Gaosheng Li ³, Mingtuan Lin ² and Li-An Bian ⁴¹ Industries Training Centre, Shenzhen Polytechnic (SZPT), Shenzhen 518055, China; dongyanfei@szpt.edu.cn² College of Electronic Science, National University of Defense Technology, Changsha 410073, China; linmingtuan08@nudt.edu.cn³ College of Electrical and Information Engineering, Hunan University, Changsha 410082, China; gaosheng@hnu.edu.cn⁴ Hunan Provincial Key Laboratory of Flexible Electronic Materials Genome Engineering, Changsha University of Science and Technology, Changsha 410004, China; dk061bianlian@126.com

* Correspondence: ydw13049059@163.com

Abstract: In this paper, a new type of terahertz (THz) metamaterial (MM) modulator has been presented with bifunctional properties based on vanadium dioxide (VO₂). The design consists of a VO₂ resonator, polyimide substrate, frequency selective surface (FSS) layer, and VO₂ film. Based on the metal-insulator transition (MIT) of VO₂, this structure integrated with VO₂ material can achieve the dynamic modulation on both transmission and reflection waves at 2.5 THz by varying the electrical conductivity value of VO₂. Meanwhile, it also exhibits adjustable absorption performance across the whole band from 0.5–7 THz. At the lower conductivity ($\sigma = 25$ S/m), this structure can act as a bandpass FSS, and, at the high conductivity ($\sigma = 2 \times 10^5$ S/m), it behaves like a wideband absorber covering 2.52–6.06 THz with absorption $A > 0.9$, which realizes asymmetric transmission. The surface electric field distributions are illustrated to provide some insight into the physical mechanism of dynamic modulation. From the simulated results, it can be observed that this design has the capability of controlling tunable manipulation on both transmission/reflection responses at a wide frequency band. This proposed design may pave a novel pathway towards thermal imaging, terahertz detection, active modulators, etc.

Keywords: metamaterial modulator; VO₂; thermal; FSS; modulation

Citation: Dong, Y.; Yu, D.; Li, G.; Lin, M.; Bian, L.-A. Terahertz Metamaterial Modulator Based on Phase Change Material VO₂. *Symmetry* **2021**, *13*, 2230. <https://doi.org/10.3390/sym13112230>

Academic Editor: Limei Qi

Received: 8 October 2021

Accepted: 10 November 2021

Published: 22 November 2021

Publisher's Note: MDPI stays neutral with regard to jurisdictional claims in published maps and institutional affiliations.



Copyright: © 2021 by the authors. Licensee MDPI, Basel, Switzerland. This article is an open access article distributed under the terms and conditions of the Creative Commons Attribution (CC BY) license (<https://creativecommons.org/licenses/by/4.0/>).

1. Introduction

In the past decade, metamaterial (MM), a kind of artificially periodic or non-periodic structure, has demonstrated outstanding electromagnetic (EM) functionalities that are not realized in natural materials such as water, soil, wood, and so on. Owing to its extraordinary EM characteristics, MM usually offers spatial potential to the asymmetric transmission in manipulating the amplitude, phase, or polarization of the incident EM waves [1–5], which enables them to be extensively studied; plentiful applications have been proposed in different regions including the polarization converter [6–8], the antenna [9–13], absorber [14–16], etc., which has greatly promoted the development of functional devices.

Currently, to control and manipulate the transmission/reflection response [17–19], a variety of active structures based on metamaterials, such as the tunable frequency selective surface (FSS) [20,21], switchable absorber [22–24], and coding metasurface [25,26], have been designed to implement the dynamic modulation performance. However, though the concept and design of active devices that are incorporated with active components (PIN diodes and varactor diodes) [27] make it possible to achieve the dynamic manipulation on the EM waves [28,29], it is not suitable for the application in the terahertz (THz) field due to the high cost and complicated manufacturing processes. At the same time, it is difficult to realize the rapid switching of absorbing, transmitting, and reflecting states in the THz regime.

To solve these problems, phase-change materials (PCM), for instance, graphene [30,31], liquid crystal [32], and vanadium dioxide (VO₂) [33], have attracted extensive attention due to their unique electromagnetic and optical performances that can be directly controlled by adopting external excitations, making them a potential new way to manipulate THz waves. Among them, VO₂ is more preferable to implement a dynamic modulation response in THz frequencies for its electrical and optical characteristics near room temperature. VO₂ can achieve an ultrafast [34] and brutal reversible metal–insulator transition (MIT) from insulator to metal provoked by thermal [35], electrical [36], or optical [37] stimuli. Although the active modulation can be faster and more efficient if excited by the electrical or optical method as compared to thermal excitation, electrical stimuli need a complex biasing network and then, the fabrication difficulty would increase significantly in the THz regime. Meanwhile, the external laser source is required for applying the optical method, making the operating system bulky and the cost high. Thus, thermal excitation is an ideal choice for modulating the property of VO₂. There is a dramatic variation in the electrical and optical performance during the phase transition (4–5 order of magnitude change on the electrical conductivity σ_{VO_2}), so VO₂ is a promising candidate in tunable MM devices at THz frequencies to achieve excellent modulation characteristics. Therefore, VO₂ is of crucial importance and can be employed in THz devices to tailor various performances. Indeed, a lot of research fields have been focused on VO₂-based tunable devices to obtain adjustable and switchable functions, such as reconfigurable THz filters [38–40], polarization converters [41–43], tunable THz absorbers [44–46], and so on. However, to the best of our knowledge, few works have been presented to achieve multiple functionalities that can be dynamically adjusted in THz devices.

In this manuscript, a novel VO₂-based THz MM modulator is proposed. By introducing the phase change material VO₂, this design can be capable of dynamically controlling the transmission/reflection response of the incident waves. When σ_{VO_2} gradually changes from 25 to 2×10^5 S/m with the external temperature increasing, the transmittance would slowly decrease from 0.89 to approximately 0 around 2.5 THz, and absorption behavior performs dynamic modulation across 0.5–7 THz. In the case of insulating state ($\sigma_{\text{VO}_2} = 25$ S/m), this structure can be used as a bandpass FSS, while when $\sigma_{\text{VO}_2} = 2 \times 10^5$ S/m, it acts as a wideband absorber over the frequency band of 2.52–6.06 THz, covering 82.5% fractional bandwidth with absorptivity of more than 0.9. The electric field distribution of this design on both top and FSS layers is provided to investigate the physical mechanism for the different states. It can be believed that this proposed design would have great potential in the applications of thermal imaging, remote sensing, and wireless communication systems, etc., due to its excellent characteristics.

2. Metamaterials (MM) Structure and Design

The three-dimensional (3D) view of the proposed unit cell geometry with a 2-dimensional (2D) array is shown in detail in Figure 1. This design is a four-layer periodic structure, which, from top to bottom, is composed of a tunable resonator designed with circle and cross geometries, polyimide substrate, bandpass FSS layer, and the ground plate. Among them, the resonator and ground plate are both symmetrical patterns and made of vanadium dioxide (VO₂) material with thicknesses of $t_1 = 0.2$ μm and $t_2 = 0.5$ μm , respectively. The dielectric constant of polyimide substrate is 3.5 with a tangent loss of $\tan \delta = 0.0027$ and a thickness (h) of 9 μm . The gold is selected as a metal model for the bandpass FSS structure with a thickness (t_2) of 0.2 μm , and a conductivity (σ) of 4.561×10^7 S/m.

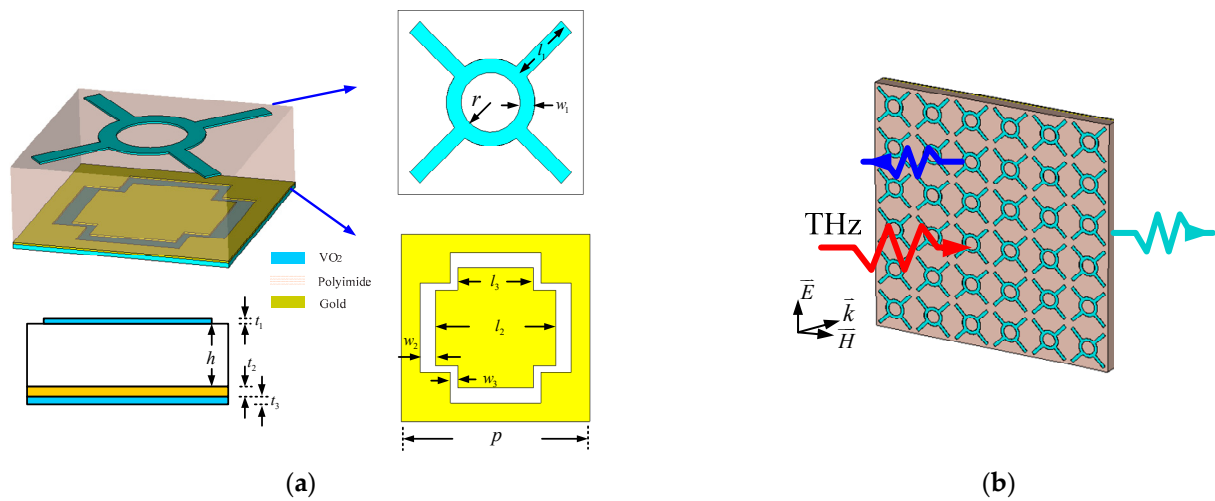


Figure 1. Unit cell of the proposed design. (a) 3D view; (b) 2D array. The parameters are (μm): $p = 25$, $l_1 = 8.5$, $l_2 = 16$, $l_3 = 10$, $w_1 = w_2 = 2$, $w_3 = 1$, $r = 4$, $h = 9$, $t_1 = t_2 = 0.2$, $t_3 = 0.5$.

During the insulator-to-metal transition of VO_2 , the conductivity value (σ_{VO_2}) can be dynamically adjusted, and its electrical characteristics will also be modulated accordingly. When the external temperature is lower (<300 K), VO_2 is in the insulating state as the insulator; as the external temperature is over 340 K [47], it would be in a metallic state like metal. According to the Bruggeman effective-medium theory, the complex dielectric properties of VO_2 can be described as follows:

$$\varepsilon_{eff} = \frac{1}{4} \left\{ \varepsilon_i(2 - 3V) + \varepsilon_m(3V - 1) + \sqrt{[\varepsilon_i(2 - 3V) + \varepsilon_m(3V - 1)] + 8\varepsilon_i\varepsilon_m} \right\} \quad (1)$$

where ε_i and ε_m are the dielectric permittivities of the insulating and metallic states of VO_2 , respectively. Additionally, V represents the volume fraction of the metallic region. When the external temperature changes, VO_2 can transform between the insulating and metallic states. ε_m can be calculated by using the Drude model:

$$\varepsilon_m(\omega) = \varepsilon_\infty - i \frac{\omega_p^2}{\omega(\omega + i/\tau)} \quad (2)$$

Here, $\varepsilon_\infty = 12$ is the dielectric permittivity at high frequency; $\tau = 5.75 \times 10^{13}$ rad/s represents the collision frequency; and $\omega_p = \sqrt{\sigma/\varepsilon_0\tau}$ denotes the plasma frequency. V can be defined as:

$$V = V_{\max} \left(1 - \frac{1}{1 + \exp[(T - T_0)/\Delta T]} \right) \quad (3)$$

where T_0 is the critical temperature of phase transition; ΔT denotes the temperature difference of the external thermal excitation between the heating and cooling processes; and V_{\max} describes the maximum limit volume distribution in the metallic state during the phase transition (≈ 0.95). Thus, based on the Equations (1)–(3), the effective conductivity of VO_2 material under different temperature cases can be expressed as:

$$\sigma_{eff}(\omega) = -i\varepsilon_0\omega(\varepsilon_{eff}(\omega) - 1) \quad (4)$$

Figure 2 illustrates the experimental results of the conductivity of VO_2 for different temperature states. From the results, it is worth noting the conductivity of VO_2 can change from 25 S/m at 300 K to 2.5×10^5 S/m at 370 K during the phase transition. When the temperature is above 350 K, the conductivity is over 2×10^5 S/m. Therefore, in simulation, the conductivity (σ_{VO_2}) of VO_2 is assumed in the range from 25 to 2×10^5 S/m.

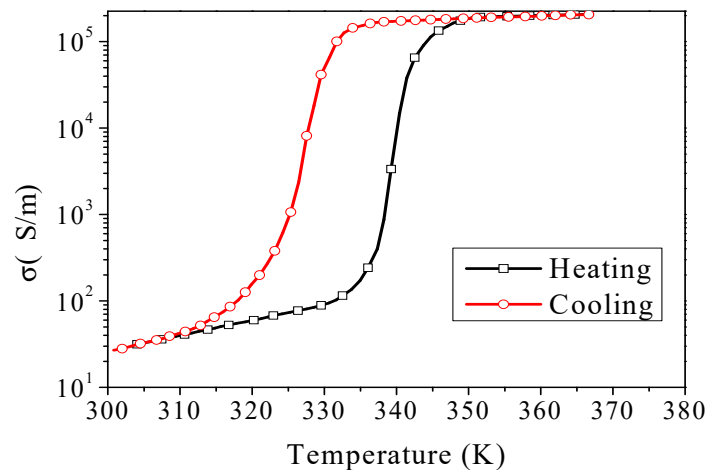


Figure 2. The measured conductivity of VO₂ under different temperature cases.

3. Results and Discussion

The numerical simulations of this design are carried out by using the commercial software CST Microwave Studio. The periodic boundary conditions are adopted along the x - and y -directions to model the infinite array. Floquet ports are used to excite the incident plane waves. Meanwhile, the absorbance $A(\omega)$ can be calculated by $A(\omega) = 1 - R(\omega) - T(\omega)$, where $R(\omega) = |S_{11}(\omega)|^2$ and $T(\omega) = |S_{21}(\omega)|^2$ represent reflectance and transmittance, respectively.

The simulated frequency responses under different conductivity values are described in Figure 3. In Figure 3a, there is a transmission peak appearing at the frequency of 2.5 THz; the transmission coefficient gradually decreases as the conductivity of VO₂ (σ_{VO_2}) increases, and when σ_{VO_2} is above 2×10^3 S/m, the transmission peak almost disappears. Then, as the value σ_{VO_2} progressively goes from 25 to 2×10^5 S/m, the transmission coefficient would slowly decrease from 0.9 to nearly 0, the amplitude modulation depth of transmission is approximately 200% at 2.5 THz, and so do the reflection results accordingly, as shown in Figure 3b,c; this obviously demonstrates that this design can achieve dynamically tunable absorption property under normal incidence across the whole frequency band of 0.5–7 THz by changing the conductivity of VO₂. There is a wide absorption bandwidth in the frequency band ranging from 2.52 to 6.06 THz with the fractional bandwidth of 82.5%, as the absorptance is more than 0.9 when $\sigma_{\text{VO}_2} = 2 \times 10^5$ S/m. However, in the insulating state ($\sigma_{\text{VO}_2} = 25$ S/m), VO₂ behaves like the insulator and the incident EM waves can transit with low insertion loss, so then this design can act as a bandpass FSS. When it is in the metallic state ($\sigma_{\text{VO}_2} = 2 \times 10^5$ S/m), VO₂ can be regarded as metal; the majority of incident EM waves would be reflected by the bottom VO₂ film, and then absorbed by the top VO₂ resonator due to ohmic loss to realize the wide absorption performance. The above results clearly indicate that this design achieves the adjustable and switchable functions by controlling the characteristics of phase transition of VO₂ material.

In an attempt to achieve a better physical insight on the working operation of this design, the electric field distributions at both top and FSS layers are investigated and shown in detail in Figure 4 at three different frequencies, in which the color refers to the intensities of the electric field.

At the frequency of 2.5 THz, from Figure 4a, the electric field is mainly distributed on the upper and lower edges of the loop-shaped aperture of the FSS layer to form the resonance and the incident waves can be allowed to pass through the structure. There exists a small part of the electric field on the top resonator, which is the reason for insertion loss at the passband. Thus, the design can produce an EM transparent window at 2.5 THz with an insertion loss as $\sigma_{\text{VO}_2} = 25$ S/m. In Figure 4b, it can be seen that the electric field is mainly focused on the four arms of the top resonator at 3.1 THz. For the frequency of 5.3 THz, an amount of the electric field is concentrated on both left and right sides of the

circle of the top layer, as illustrated in Figure 4c. The electric field distributions indicate that the absorption mainly comes from the ohmic dissipation of the top VO₂ resonator when $\sigma_{\text{VO}_2} = 2 \times 10^5$ S/m for these two frequencies.

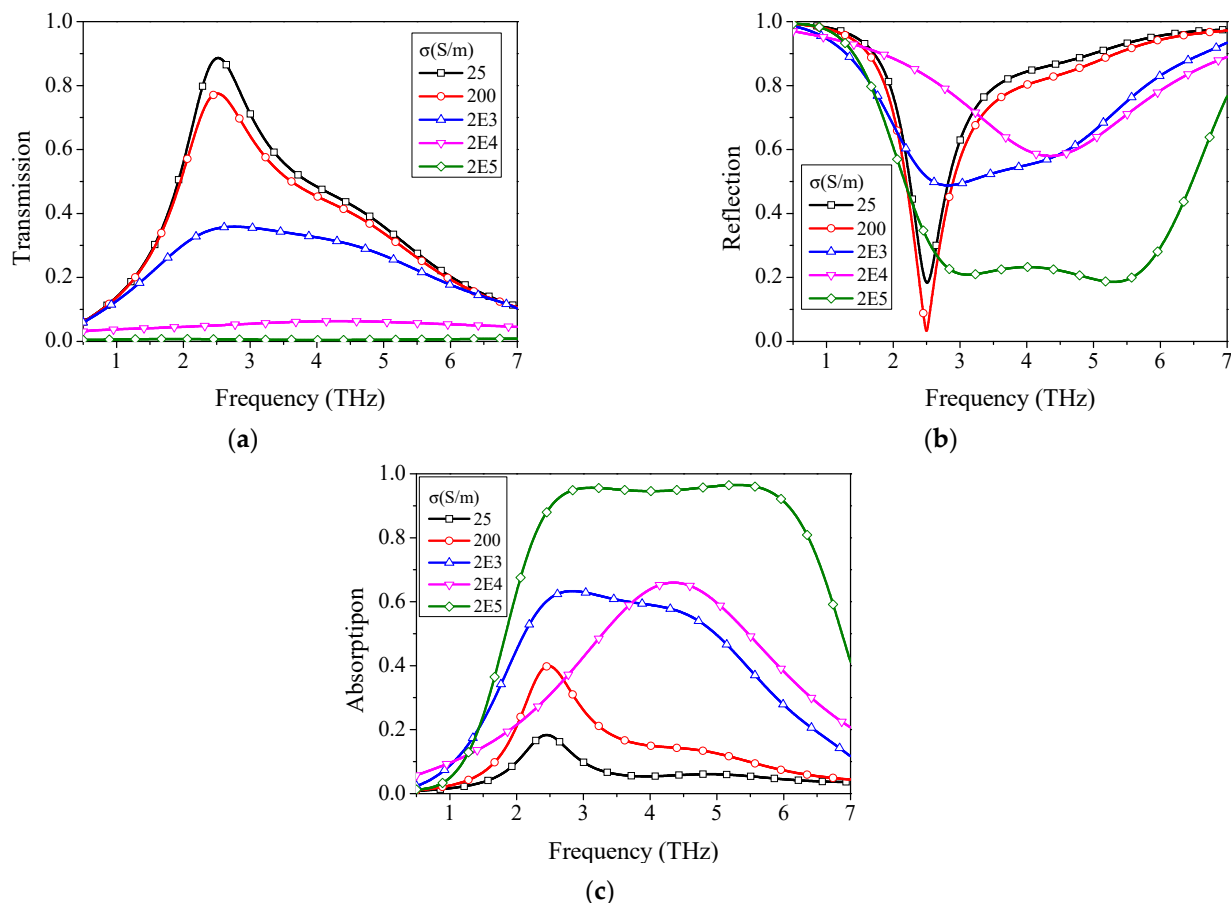


Figure 3. The simulated results of this design for different conductivity states: (a) transmission; (b) reflection; (c) absorption.

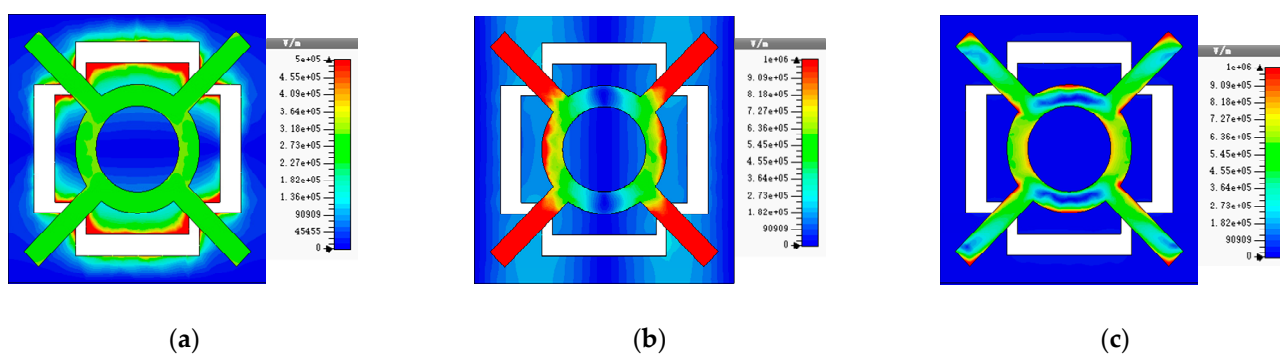


Figure 4. The electric field distributions on the top and FSS layers at (a) 2.5 THz, (b) 3.1 THz, and (c) 5.3 THz, respectively.

As a result, the proposed configuration incorporated with VO₂ material generates a highly effective modulation performance on the transmission/reflection response. It demonstrates that the transmission/reflection modulation located at 2.5 THz and the tunable absorption property is implemented simultaneously by applying phase-change material VO₂.

Figure 5 depicts the oblique incidence properties for two different conductivity states in both cases of TE and TM polarizations. From the above results, it is seen that this design maintains relatively robust angular stability at the passband of 2.5 THz over the incident

angle (θ , the angle between the incident wave vector \vec{k} and the z -axis), ranging from 0° to 45° for both TE and TM waves in Figure 5a,b with $\sigma_{\text{VO}_2} = 25 \text{ S/m}$. However, some harmonics are appearing at the higher frequencies for both cases, as θ is greater than 15° , which is attributed to the mutual coupling between adjacent units. Figure 5c,d describes the absorption responses against the incident angle (θ) as $\sigma_{\text{VO}_2} = 2 \times 10^5 \text{ S/m}$. In TE mode, the absorption gradually deteriorates when θ goes up to 45° at the lower absorption band with the absorbance > 0.8 , as plotted in Figure 5c. It can be ascribed to the fact that the parallel E -field component gradually decreases with increasing θ . On the contrary, the absorption performance almost remains stable even though θ reaches up to 45° for the TM mode because the parallel E -field component stays nearly unchanged. From the above results, for the TM mode, the design has good angular stability on absorption performance as compared with that in the TE mode when θ increases up to 45° , as detailed in Figure 5d.

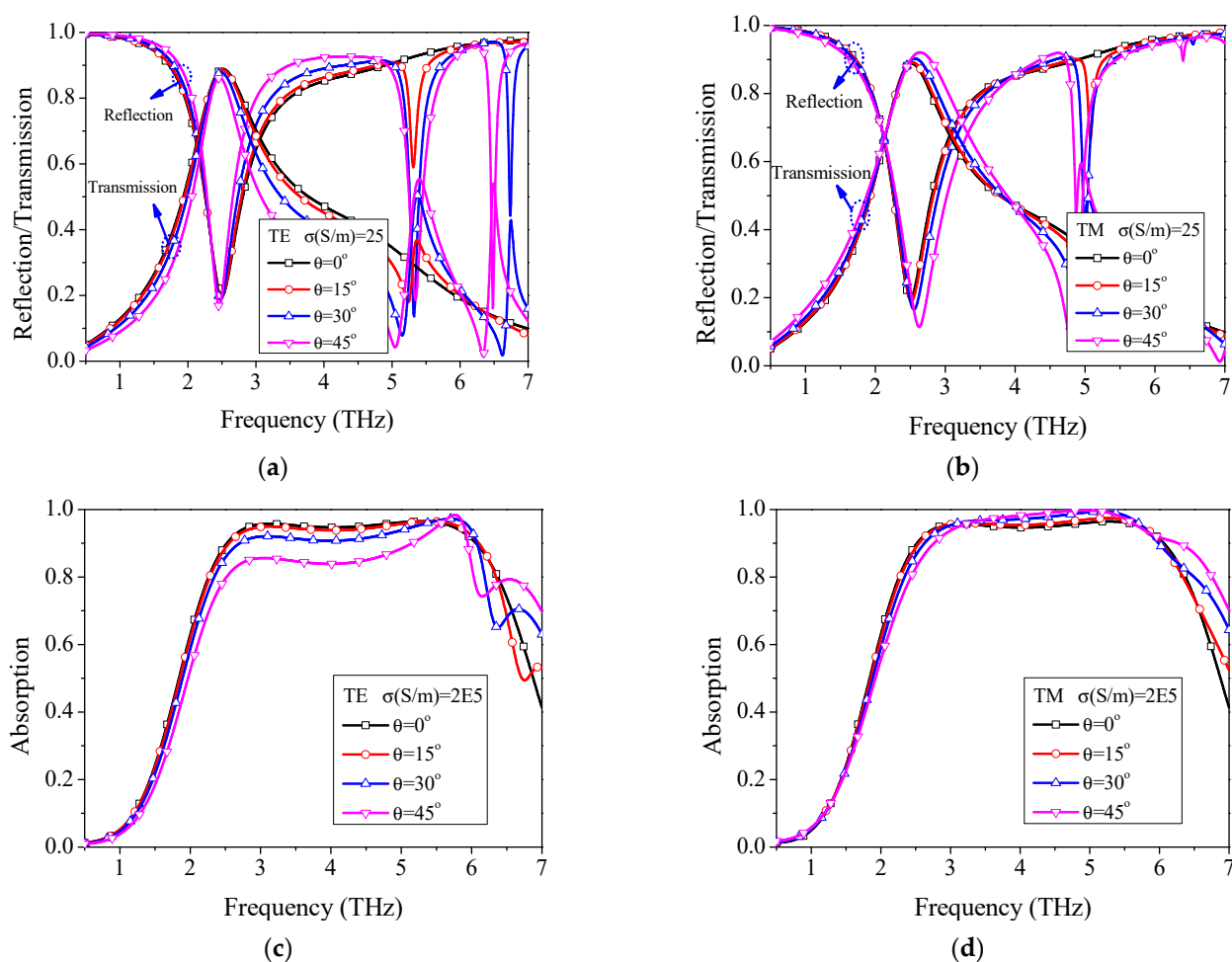


Figure 5. The transmission/reflection and absorption performances under different incident angles under (a,c) TE and (b,d) TM modes for different conductivity states.

4. Conclusions

In conclusion, a tunable THz MM modulator with bifunctional properties integrated with VO_2 has been presented in the article. By utilizing the phase transition performance of VO_2 from the insulator to metal, the proposed design can realize the dynamic manipulation of the incident THz waves. Compared to the previous works, this design has high modulation characteristics for the transmission/reflection and absorption responses. With the conductivity σ_{VO_2} changing from 25 to $2 \times 10^5 \text{ S/m}$, the design provides high modulation depth on the transmission/reflection at the frequency of 2.5 THz, and achieves

the tunable absorption performance over the whole frequency band of 0.5–7 THz. At the lower conductivity ($\sigma_{\text{VO}_2} = 25 \text{ S/m}$), this design can be used as the bandpass FSS, while also acting as a wider absorber across the operating frequency band ranging from 2.52–6.06 THz with the absorption of over 0.9 and fractional bandwidth of 82.5% as $\sigma_{\text{VO}_2} = 2 \times 10^5 \text{ S/m}$. In addition, it still possesses the polarization-insensitivity performance for structural symmetry. The design demonstrates attractive advantages, which paves a new way towards the THz modulator with asymmetric transmission property, and may be extensively applied to biological imaging, thermal scanning, THz camouflage, etc.

Author Contributions: This study was conducted through the contributions of all authors. Conceptualization, investigation, validation, writing—original draft preparation, D.Y. and Y.D.; software, writing—review and editing, G.L. and M.L.; visualization, supervision, L.-A.B. All authors have read and agreed to the published version of the manuscript.

Funding: This work was supported by the Young Creative Talents Project of Guangdong Provincial Department of Education under Grant No. 2020KQNCX203.

Conflicts of Interest: The authors declare no conflict of interest.

References

1. Huang, X.; Yang, F.; Gao, B.; Yang, Q.; Wu, J.; He, W. Metamaterial absorber with independently tunable amplitude and frequency in the terahertz regime. *Opt. Express* **2019**, *27*, 25902–25911. [[CrossRef](#)]
2. Liu, C.; Liu, P.; Yang, C.; Lin, Y.; Liu, H. Analogue of dual-controlled electromagnetically induced transparency based on a graphene metamaterial. *Carbon* **2019**, *142*, 354–362. [[CrossRef](#)]
3. Davis, T.J.; Gómez, D.E.; Eftekhari, F. All-optical modulation and switching by a metamaterial of plasmonic circuits. *Opt. Lett.* **2014**, *39*, 4938–4941. [[CrossRef](#)]
4. Huang, W.X.; Zhao, G.R.; Guo, J.J.; Wang, M.S.; Shi, J.P. Nearly perfect absorbers operating associated with fano resonance in the infrared range. *Chin. Phys. Lett.* **2016**, *33*, 088103. [[CrossRef](#)]
5. Guo, Y.; Yan, L.; Pan, W.; Shao, L. Scattering engineering in continuously shaped metasurface: An approach for electromagnetic illusion. *Sci. Rep.* **2016**, *6*, 30154. [[CrossRef](#)]
6. Zhang, Z.; Cao, X.; Gao, J.; Li, S. Broadband metamaterial reflectors for polarization manipulation based on cross/ring resonators. *Radioengineering* **2016**, *25*, 436–441. [[CrossRef](#)]
7. Zhang, Y.; Feng, Y.; Jiang, T.; Cao, J.; Zhao, J.; Zhu, B. Tunable broadband polarization rotator in terahertz frequency based on graphene metamaterial. *Carbon* **2018**, *133*, 170–175. [[CrossRef](#)]
8. Zarrabi, F.B.; Pirooj, A.; Pedram, K. Metamaterial loads used in microstrip antenna for circular polarization. *Int. J. RF Microw. Comput.-Aided Eng.* **2019**, *29*, e21869. [[CrossRef](#)]
9. Wang, W.; Zheng, Z.; Fang, X.; Zhang, H.; Jin, M.; Lu, J.; Luo, Q.; Gao, S. A waveguide slot filtering antenna with an embedded metamaterial structure. *IEEE Trans. Antennas Propag.* **2019**, *67*, 2953–2960. [[CrossRef](#)]
10. Yan, S.; Vandenbosch, G.A.E. Radiation pattern-reconfigurable wearable antenna based on metamaterial structure. *IEEE Antennas Wirel. Propag. Lett.* **2016**, *15*, 1715–1718. [[CrossRef](#)]
11. Li, X.; Zhou, H.; Gao, Z.; Wang, H.; Lv, G. Metamaterial slabs covered UWB antipodal Vivaldi antenna. *IEEE Antennas Wirel. Propag. Lett.* **2017**, *16*, 2943–2946. [[CrossRef](#)]
12. Labidi, M.; Choubani, F. Performances enhancement of metamaterial loop antenna for terahertz applications. *Opt. Mater.* **2018**, *82*, 116–122. [[CrossRef](#)]
13. Lin, M.; Xu, M.; Wan, X.; Liu, H.; Wu, Z.; Liu, J.; Deng, B.; Guan, D.; Zha, S. Single sensor to estimate DOA with programmable metasurface. *IEEE Internet Things J.* **2021**, *8*, 10187–10197. [[CrossRef](#)]
14. Cen, C.; Yi, Z.; Zhang, G.; Zhang, Y.; Liang, C.; Chen, X.; Tang, Y.; Ye, X.; Yi, Y.; Wang, J.; et al. Theoretical design of a triple-band perfect metamaterial absorber in the THz frequency range. *Results Phys.* **2019**, *14*, 102463. [[CrossRef](#)]
15. Zhou, Y.; Xia, H.; Zhang, L.; Zhao, Y.; Xie, W. Temperature insensitive ultra-broadband THz metamaterial absorber based on metal square ring resonators. *Results Phys.* **2021**, *22*, 103915. [[CrossRef](#)]
16. Chen, J.; Yang, M.-S.; Li, Y.-D.; Cheng, D.-K.; Guo, G.-L.; Jiang, L.; Zhang, H.-T.; Song, X.-X.; Ye, Y.-X.; Ren, Y.-P.; et al. Tunable terahertz wave broadband absorber based on metamaterial. *Acta Phys. Sin.* **2019**, *68*, 247802. [[CrossRef](#)]
17. Liu, Y.; Yang, H.; Huang, X.; Yu, Z.; Li, S.; Yang, Y. A metamaterial polarization converter with half reflection and half transmission simultaneously. *Phys. Lett. A* **2021**, *389*, 127101. [[CrossRef](#)]
18. Yu, X.; Gao, X.; Qiao, W.; Wen, L.; Yang, W. Broadband tunable polarization converter realized by graphene-based metamaterial. *IEEE Photonics Technol. Lett.* **2016**, *28*, 2399–2402. [[CrossRef](#)]
19. Xiao, Z.; Zou, H.; Zheng, X.; Wen, L.; Yang, W. A tunable reflective polarization converter based on hybrid metamaterial. *Opt. Quantum Electron.* **2017**, *49*, 401. [[CrossRef](#)]

20. Bai, H.; Yan, M.B.; Li, W.H.; Wang, J.F.; Zheng, L.; Wang, H.; Qu, S.B. Tunable frequency selective surface with angular stability. *IEEE Antennas Wirel. Propag. Lett.* **2021**, *20*, 1108–1112. [[CrossRef](#)]
21. Guo, Q.X.; Zhao, Z.Q.; Su, J.X.; Li, Z.R. Dual-polarization absorptive/transmissive frequency-selective surface with tunable passband. *IEEE Trans. Electromagn. Compat.* **2021**, *63*, 1347–1356. [[CrossRef](#)]
22. Li, H.; Costa, F.; Wang, Y.; Cao, Q.; Monorchio, A. A switchable and tunable multifunctional absorber/reflector with polarization-insensitive features. *Int. J. RF Microw. Comput.-Aided Eng.* **2021**, *31*, e22573. [[CrossRef](#)]
23. Ghosh, S.; Srivastava, K.V. Polarization-insensitive single-and broadband switchable absorber/reflector and its realization using a novel biasing technique. *IEEE Trans. Antennas Propag.* **2016**, *64*, 3665–3670. [[CrossRef](#)]
24. Qu, M.; Chang, T.; Guo, G.; Li, S. Design of graphene-based dual-polarized switchable absorber/absorber at terahertz. *IEEE Access* **2020**, *8*, 127220–127225. [[CrossRef](#)]
25. Liu, S.; Cui, T.J.; Xu, Q.; Bao, D.; Du, L.; Wan, X.; Tang, W.; Ouyang, C.; Zhou, X.; Yuan, H.; et al. Anisotropic coding metamaterials and their powerful manipulation of differently polarized terahertz waves. *Light Sci. Appl.* **2016**, *5*, e16076. [[CrossRef](#)]
26. Liu, S.; Zhang, L.; Cu, T.J.; Yang, Q.L.; Xu, Q.; Yang, Y.; Noor, A.; Zhang, Q.; Iqbal, S.; Wan, X.; et al. Frequency-dependent dual-functional coding metasurfaces at terahertz frequencies. *Adv. Opt. Mater.* **2016**, *4*, 1965–1973. [[CrossRef](#)]
27. Pan, S.; Lin, M.; Xu, M.; Zhu, S.; Bian, L.A.; Li, G. A low-profile programmable beam scanning holographic array antenna without phase shifters. *IEEE Internet Things J.* **2021**. [[CrossRef](#)]
28. Fang, J.; Huang, J.; Gou, Y.; Shang, Y. Research on broadband tunable metamaterial absorber based on PIN diode. *Optik* **2020**, *200*, 163171. [[CrossRef](#)]
29. Luo, Y.; He, Y.; Xu, S.; Yang, G. Programmable zeroth-order resonance with uniform manipulation using the nonlinearity of PIN diodes. *IEEE Antennas Wirel. Propag. Lett.* **2019**, *18*, 2419–2423. [[CrossRef](#)]
30. Jiang, H.; Cui, Y.; Jiang, Y. Two-dimensional tunable polarization-dependent absorptions for binary and ternary coding. *Opt. Mater. Express* **2020**, *10*, 787–795. [[CrossRef](#)]
31. Liu, W.; Song, Z. Terahertz absorption modulator with largely tunable bandwidth and intensity. *Carbon* **2021**, *174*, 617–624. [[CrossRef](#)]
32. He, X.; Shi, S.; Yang, X.; Li, S.; Wu, F.; Jiang, J. Voltage-tunable terahertz metamaterial based on liquid crystal material for bandpass filters and phase shifters. *Integr. Ferroelectr.* **2017**, *178*, 131–137. [[CrossRef](#)]
33. Song, Z.; Zhang, J. Achieving broadband absorption and polarization conversion with a vanadium dioxide metasurface in the same terahertz frequencies. *Opt. Express* **2020**, *28*, 12487–12497. [[CrossRef](#)]
34. Jeong, Y.G.; Bahk, Y.M.; Kim, D.S. Dynamic terahertz plasmonics enabled by phase-change materials. *Adv. Opt. Mater.* **2020**, *8*, 1900548. [[CrossRef](#)]
35. Hashemi, M.R.M.; Yang, S.H.; Wang, T.; Sepúlveda, N.; Jarrahi, M. Electronically-controlled beam-steering through vanadium dioxide metasurfaces. *Sci. Rep.* **2016**, *6*, 35439. [[CrossRef](#)] [[PubMed](#)]
36. Shin, J.H.; Park, K.H.; Ryu, H.C. Electrically controllable terahertz square-loop metamaterial based on VO₂ thin film. *Nanotechnology* **2016**, *27*, 195202. [[CrossRef](#)] [[PubMed](#)]
37. Coy, H.; Cabrera, R.; Sepúlveda, N.; Fernández, F. Optoelectronic and all-optical multiple memory states in vanadium dioxide. *J. Appl. Phys.* **2010**, *108*, 113115. [[CrossRef](#)]
38. Zhao, S.; Hu, F.; Xu, X.; Jiang, M.; Zhang, W.; Yin, S.; Jiang, W. Electrically triggered dual-band tunable terahertz metamaterial band-pass filter based on Si₃N₄-VO₂-Si₃N₄ sandwich. *Chin. Phys. B* **2019**, *28*, 054203. [[CrossRef](#)]
39. Sanphuang, V.; Ghalichechian, N.; Nahar, N.K.; Volakis, J.L. Reconfigurable THz filters using phase-change material and integrated heater. *IEEE Trans. Terahertz Sci. Technol.* **2016**, *6*, 583–591. [[CrossRef](#)]
40. Li, T.; Luo, X.; Hu, F.; Li, G.; Xu, W.; Zhou, Y.; Wang, Z.; Zhang, X.; Zhang, L.; Wang, Y. Terahertz bandstop-to-bandpass converter based on VO₂ hybrid metasurface. *J. Phys. D Appl. Phys.* **2021**, *54*, 435105. [[CrossRef](#)]
41. Yahiaoui, R.; Chase, Z.A.; Kyaw, C.; Seabron, E.; Mathews, J.; Searles, T.A. Dynamically tunable single-layer VO₂/metasurface based THz cross-polarization converter. *J. Phys. D Appl. Phys.* **2021**, *54*, 235101. [[CrossRef](#)]
42. Yang, C.; Gao, Q.; Dai, L.; Zhang, Y.; Zhang, H.; Zhang, Y. Bifunctional tunable terahertz circular polarization converter based on Dirac semimetals and vanadium dioxide. *Opt. Mater. Express* **2020**, *10*, 2289–2303. [[CrossRef](#)]
43. Lv, F.; Wang, L.; Xiao, Z.; Chen, M.; Cui, Z.; Xu, Q. Asymmetric transmission polarization conversion of chiral metamaterials with controllable switches based on VO₂. *Opt. Mater.* **2021**, *114*, 110667. [[CrossRef](#)]
44. Zhao, Y.; Huang, Q.; Cai, H.; Lin, X.; Lu, Y. A broadband and switchable VO₂-based perfect absorber at the THz frequency. *Opt. Commun.* **2018**, *426*, 443–449. [[CrossRef](#)]
45. Ren, Z.; Cheng, L.; Hu, L.; Liu, C.; Jiang, C.; Yang, S.; Ma, Z.; Zhou, C.; Wang, H.; Zhu, X. Photoinduced broad-band tunable terahertz absorber based on a VO₂ thin film. *ACS Appl. Mater. Interfaces* **2020**, *12*, 48811–48819. [[CrossRef](#)] [[PubMed](#)]
46. Zhang, Y.; Wu, P.; Zhou, Z.; Chen, X.; Yi, Z.; Zhu, J.; Zhang, T.; Jile, H. Study on temperature adjustable terahertz metamaterial absorber based on vanadium dioxide. *IEEE Access* **2020**, *8*, 85154–85161. [[CrossRef](#)]
47. Song, Z.; Wang, K.; Li, J.; Liu, Q.H. Broadband tunable terahertz absorber based on vanadium dioxide metamaterials. *Opt. Express* **2018**, *26*, 7148–7154. [[CrossRef](#)] [[PubMed](#)]